Catalysis Today 140 (2009) 149–156

Contents lists available at ScienceDirect

Catalysis Today

journal homepage: www.elsevier.com/locate/cattod

Intensified Fischer–Tropsch synthesis process with microchannel catalytic reactors

Chunshe Cao, Jianli Hu, Shari Li, Wayne Wilcox, Yong Wang *

Institute for Interfacial Catalysis, Pacific Northwest National Laboratory, 902 Battelle Blvd, Richland, WA 99354, United States

ARTICLE INFO

Article history:
Available online 5 December 2008

Keywords:
Gas to liquid
Fischer–Tropsch synthesis
Cobalt–Rhenium catalyst
Alumina support
Microchannel reactor
Particle size
Temperature profiles

ABSTRACT

A microchannel catalytic reactor with improved heat and mass transport has been used for Fischer–Tropsch synthesis. It was demonstrated that this microchannel reactor based process can be carried out at gas hourly space velocity (GHSV) as high as 60,000 h^{-1} to achieve greater than 60% of single-pass CO conversion while maintaining relatively low methane selectivity (<10%) and high chain growth probability (>0.9). In this study, performance data were obtained over a wide range of pressure (10–35 atm) and hydrogen-to-carbon monoxide ratio (1–2.5). The catalytic materials were characterized using BET, scanning electron microcopy (SEM), transmission electron microcopy (TEM), and H_2 chemisorption. A three-dimensional pseudo-homogeneous model was used to simulate temperature profiles in the exothermic reaction system in order to optimize the reactor design. Intraparticle non-isothermal characteristics are also analyzed for the FT synthesis catalyst.

© 2008 Elsevier B.V. All rights reserved.

1. Introduction

Gas to liquid conversion via Fischer–Tropsch synthesis is a viable strategy to monetize stranded natural gas and salvage associated gas while meeting environmental specifications and maintaining pipeline productivity [1–6]. Co based catalysts are known as active and selective in the conversion of syngas to hydrocarbon fuels [7–11]. In conventional FT synthesis processes, three types of reactors including fixed bed reactor, circulating and entrained fluidized bed reactor, and slurry reactor, have been used [12–15]. Advantages and drawbacks of each reactor types have been well studied in the last 60 years' industrial practice [12–23]. It is demonstrated that the product composition characterized by the chain growth probability, α, is determined mainly by the catalyst, process conditions, and type of reactor. Among many factors that influence product selectivity, temperature control is the most important, as hot spots in a fixed bed significantly promote methane formation, decrease α and deactivate the catalyst. In this paper, a microchannel reactor, which has advanced heat and mass characteristics [24–26], was used to evaluate the potential space time yield improvement of a supported cobalt catalyst under improved heat transfer regions.

2. Experimental

Experiments were carried out in a microchannel reactor system with active cooling to maintain isothermal conditions in the catalyst bed. This reactor has a built-in preheating zone with catalyst bed temperature measurement capabilities. Fig. 1 shows schematics of the reactor assembly. The catalytic portion of the reactor is a microchannel slot with the gap width of 0.508 mm and the details of this reactor are described elsewhere [27]. The catalyst is located in the lower portion of the channel so that the reactant gases can be preheated to a desired temperature in the upper portion of the channel before entering the catalyst bed. The microchannel is "sandwiched" by two separated oil-heating/cooling channels, which are designed to allow oil to circulate at a high rate to achieve a high heat transfer coefficient.

A schematic of the reactor unit setup is shown in Fig. 2. Pretreatment gases and other reactant gases can be precisely controlled and delivered into the reactor using mass flow controllers. Reactor effluent is quenched, and liquid products are collected in a chilled vessel which is kept at 0 °C. Non-condensable gaseous products such as CO, H_2 and CH_4 are analyzed by a micro-gas chromatograph (GC) (Agilent QUADH G2891A) to determine conversion and selectivity to light products. The micro-GC is equipped with Molsieve 5A (10 m), PoraPlotQ (8 m), OV-1 (2 μm, 10 m) and OV-1 (1.2 μm, 4 m) columns to quantify carbon monoxide, carbon dioxide, hydrogen, methane, ethane, ethylene, propane, and propylene. With N_2 tracer in the reactant mixture as

* Corresponding author.
E-mail address: yongwang@pnl.gov (Y. Wang).

0920-5861/$ – see front matter © 2008 Elsevier B.V. All rights reserved.
doi:10.1016/j.cattod.2008.10.016

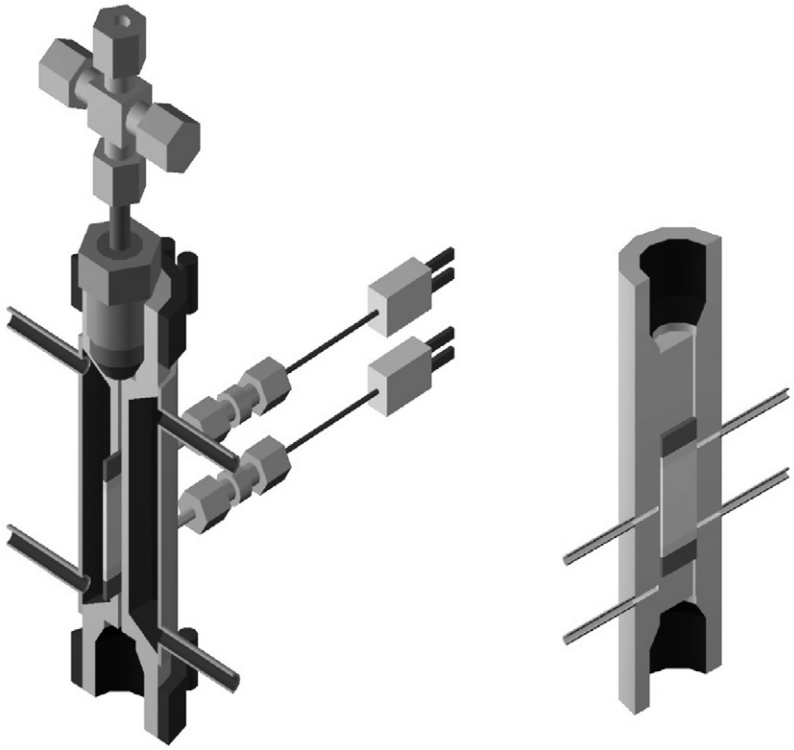

Fig. 1. Reactor assembly.

an internal standard, combined with measured gas inlet and outlet flowrates and compositions, the overall material balance is better than 98%. The system pressure is controlled by a backpressure regulator (BPR). All process data, such as temperature, pressure, and flowrates, are recorded with a LabView 6.2 data acquisition system in a computer and displayed in real time. Four thermal couples along the catalyst bed indicated that the temperature gradient along the catalyst bed is less than 1 °C under the targeted reaction temperature.

Two powdered 30 wt.% Co/4.5 wt.% Re/γ-Al_2O_3 catalysts with different particle sizes (45 and 150 μm) were prepared using a multi-step incipient-wetness impregnation method with an inter-calcination protocol. γ-Al_2O_3 (Sasol Puralox) was pre-treated at 500 °C in air for 2 h prior to the impregnation. The support has spherical shape and uniform particle distribution. An aqueous solution of cobalt nitrate hexahydrate ($Co(NO_3)_2{\cdot}6H_2O$) (98% purity, Aldrich) and Perrhenic acid ($HReO_4$) (Engelhard, 53.29 wt.% P.M.) was impregnated onto the γ-Al_2O_3 support in a crucible dish. The sample was shaken for 15 min before being dried in air at 90 °C for 8 h. The sample was then calcined at 350 °C in air for 3 h. Five sequential incipient-wetness impregnations were used with the pore volume adjusted after each calcination. The final catalyst has a surface area of 60 m^2/g and a pore volume of 0.14 cm^3/g.

0.2 g catalyst particles were packed in the microreactor. The catalyst was activated in situ with two redox cycles and each cycle consisted of two steps: in the first step, the catalyst is reduced with 10% H_2 in helium. The temperature was ramped to 250 °C at a 0.5 °C/min and held for half an hour. Then the catalyst was heated up to 400 °C at a 0.5 °C/min and held for 10 h. Helium was introduced before the reactor was cooled down to room temperature. In step 2, the catalyst was oxidized with 2% O_2 in Helium. The reactor was heated at a ramping rate of 2 °C/min to 350 °C and held for 2 h. Helium purge is introduced before cooling. Both steps were repeated to complete the two redox cycles. The final reduction was conducted by raising the temperature to 400 °C at 0.5 °C/min with 10% H_2 in helium and holding at 400 °C for 12 h. The temperature was then dropped to 160 °C and the reactor was pressurized with 10% H_2 in helium and switched to the hydrogen and carbon monoxide mixture. The hydrogen and carbon monoxide used for synthesis is premixed with 4% nitrogen as an internal standard. The reactor was ramped to the target temperature at 0.1 °C/min, and the activity data were taken at least after 72 h TOS when the system reached steady state. The liquid wax products are analyzed offline with HP GC (5890). The GC is configured with a DB5 column of 15 m long, 0.32 mm i.d., 0.25 μm film thickness, which is connected to a flame ionization detector (FID). Data acquisition and control is performed by Chemstation software. The aqueous phase containing water, alcohols, ketones, etc. is first extracted out and washed with methylene chloride several times. The liquid wax mixture is sonicated and dissolved with cyclohexane in a volumetric flask before being further diluted. For a typical product analysis, the GC oven program is set as: initial 40 °C for 1.5 min, then 5 °C/min ramp to final temperature of 350 °C, held for 7 min.

3. Results and discussions

3.1. Catalytic performance of Co/Re/Al_2O_3 catalysts

Fig. 3 shows SEM pictures of the two catalysts with different particle sizes (150 and 45 μm). It can be seen that the formulated catalysts are highly spherical and have narrow particle size distributions. They also exhibit smooth surfaces with fewer edges for minimal fine formation. The metal dispersion was measured to be 5.6% that is comparable to the literature reported value at a lower Co loading (e.g. 20 wt.%) [7]. Experimental results show a high cobalt-time-yield (mole CO converted/g-atom total Co-s) of

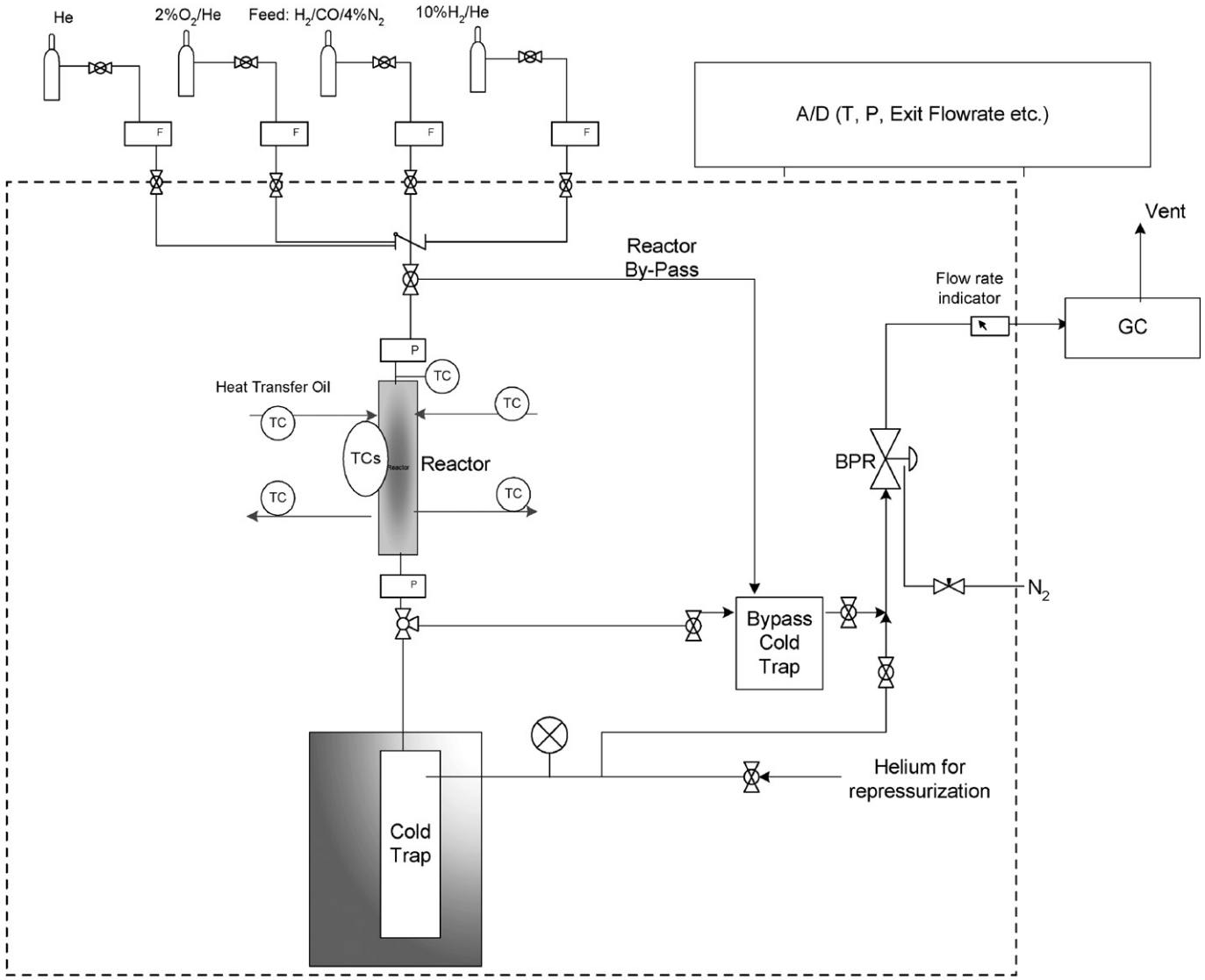

Fig. 2. Schematic of reactor system process diagram. F: mass flow controller; P: pressure transducer; TC: thermocouple; A/D: analog/digital data acquisition; BPR: back pressure regulator.

6.17×10^{-3} s^{-1} at 220 °C and 20 atm with a GHSV of 21,500 h^{-1} even at a high Co loading of 30%.

Table 1 shows productivity comparison of these two catalysts. Catalyst with a smaller particle size exhibited a lower methane selectivity and higher productivity at the same pressure (25 atm). Improved productivities as high as 2.14 g C_{2+}/(g-cat h) were also observed with these two catalysts in a microchannel reactor which are higher than those typically reported in the literature (~0.5 g C_{2+}/(g-cat h)). The improved productivity was due in part to a better temperature control in a microchannel reactor which allows the operation under a higher gas hourly space velocity (GHSV).

Pressure effects on the Fischer–Tropsch synthesis for the catalyst with a smaller particle size are shown in Fig. 4. The reactor was operated at different operating pressures with the same temperature (224 °C) and weight hourly space velocity (WHSV = 4.92 g CO/(g-cat h)) that corresponds to 21,500 h^{-1} GHSV. Results show that the CH_4 selectivity can be reduced from 12% to 3.4% when the system pressure increases from 10 to 35 atm. The CO conversion increased from 50% to 90% due to a higher

Table 1
Productivity comparison.

Catalyst Co/Re = 21 (atomic ratio)	Co (wt.%)	P (atm)	GHSV (h^{-1})	WHSV (g CO/(g-cat h))	CO conversion (%)	CH_4 selectivity (%)	α	Productivity (g C_{2+}/(g-cat h))	Productivity (g C_{2+}/(g-Co h))
Catalyst A (150 μm powder)	30	10	20,016	4.9126	48.6	22.8	0.81	0.92	3.0726
		25		4.9126	62.6	16.7	0.86	1.28	4.2728
Catalyst B (45 μm powder)	30	25	22,886	4.9126	76.8	10.7	0.88	1.69	5.6301
		35		4.9126	90.2	3.4	0.92	2.14	7.1180

T = 224 °C, H_2/CO = 2.

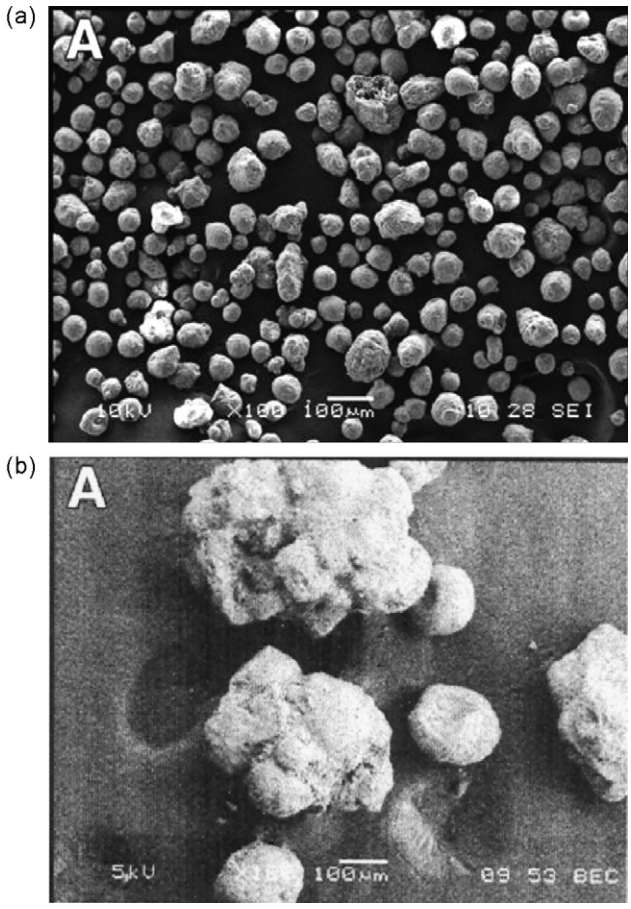

Fig. 3. SEM micrographs of 30 wt.% Co/4.5 wt.% Re/Al_2O_3 catalysts. (a) d_p = 45 μm and (b) d_p = 150 μm.

reactant partial pressure and a longer residence time at 35 atm (GHSV is defined as the inlet gas flowrate at standard temperature and pressure divided by the catalyst bed volume). Analysis of liquid/wax sample showed that the chain growth probability (α) also increases with pressure. Therefore, high-pressure operation significantly reduces methane formation and improves the middle distillates and wax selectivity.

The effects of H_2/CO ratio were experimentally studied. Fig. 5 shows that at the same process conditions (T, P, WHSV), CO conversion increases with increase of H_2/CO ratio, while methane selectivity increases and the chain growth probability (α) decreases. This is due to the fact that the increased hydrogen

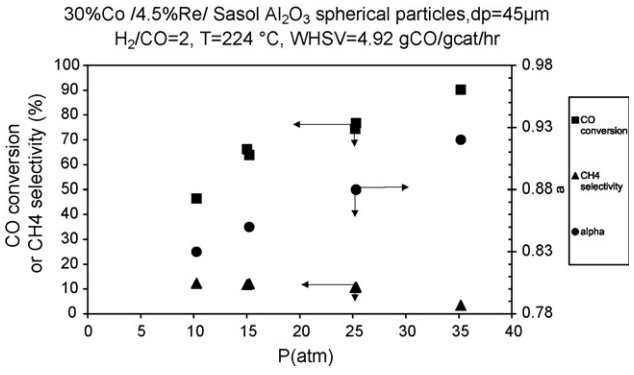

Fig. 4. Pressure effects on Fischer–Tropsch synthesis.

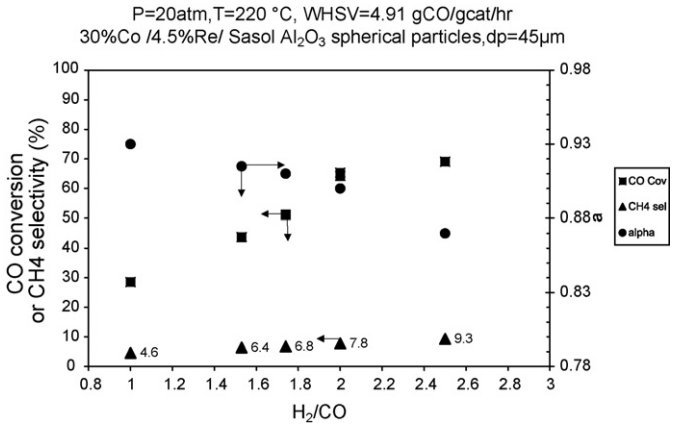

Fig. 5. H_2/CO ratio effects on Fischer–Tropsch synthesis.

partial pressure at high H_2/CO ratio accelerates the reaction rate since FT synthesis reaction kinetics has a positive order to hydrogen partial pressure [7,12,23,28,29]. In the meantime, the high hydrogen concentration on the catalyst sites also results in fast methanation rate.

The above catalyst performance shows that FT synthesis process can be intensified by using the highly active and selective Co catalyst in a microchannel reactor which provides effective heat and mass transfer characteristics. Fig. 6 shows that 63% CO conversion has been achieved with a methane selectivity of ~10.5% when the reactor is operated at 60,000 h^{-1} GHSV, 20 atm and 235 °C. This GHSV is about 15 times faster than that in Shell's conventional fixed bed technology [13]. The catalyst life is notably stable at above conditions. For about 500 h operation, the catalyst deactivation rate constant was found to be 0.0055 day^{-1}.

Representative TEM micrograph of a redox treated $Co/Re/Al_2O_3$ catalyst is shown in Fig. 7. An average Co particle size of 4 nm was observed with the TEM characterization in the high Co loading (30%) catalyst (Fig. 7a), which is smaller than the measurement from chemisorption probably due to incomplete reduction of Co when supported on alumina support. The micrograph of a spent catalyst after exposure to reactants at 232 °C for 1000 h is shown in Fig. 7b. It can be seen that some of the metal particles segregate on the support matrix to form large particles (~30–40 nm). Analysis of the dispersed area versus segregated area using energy dispersive X-ray spectroscopy (EDS/EDX) also shows that the

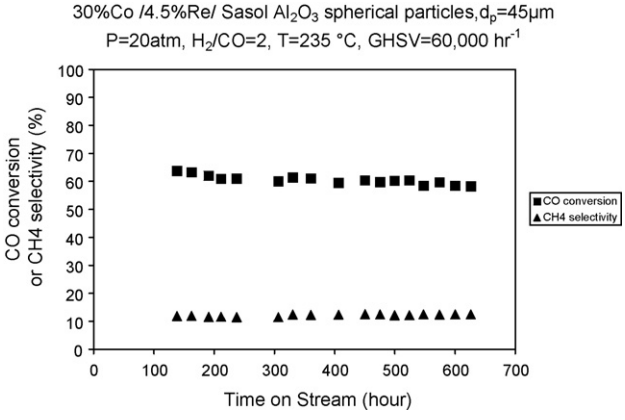

Fig. 6. Catalytic performance of an intensified FT synthesis process using the selective Co catalyst with increased site density in a microchannel reactor.

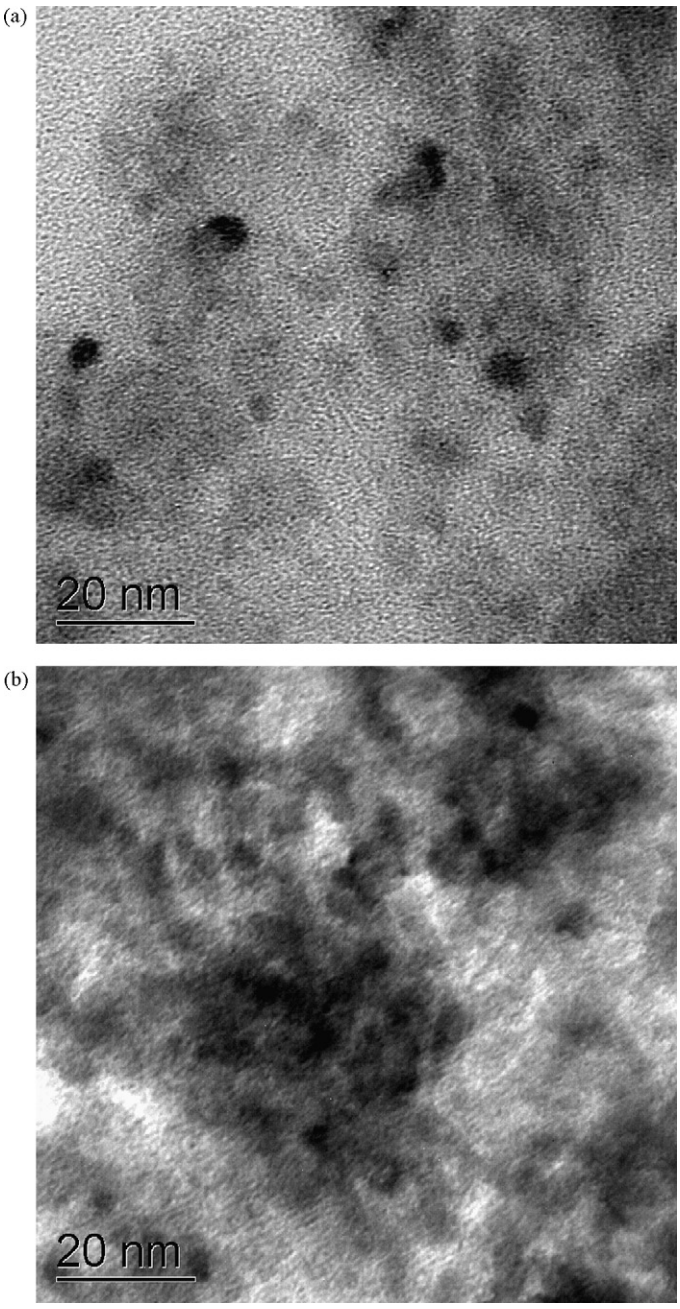

Fig. 7. High-resolution TEM micrographs of $Co/Re/Al_2O_3$ catalysts. (a) 30 wt.% Co/4.5 wt.% Re/Al_2O_3. (b) Spent sample: 30 wt.% Co/4.5 wt.% Re/Al_2O_3 after Fischer–Tropsch synthesis reactions at 232 °C for 1000 h.

Co/Al atomic ratio increases dramatically from 0.37 to 1.87 indicating the metal particles agglomerate to a great extent (Fig. 8). This reveals in part the catalyst deactivation mechanism.

3.2. Reactor and catalyst modeling

For a strongly exothermic reaction such as FT synthesis, temperature control is critical in minimizing methanation and prolonging catalyst life. In order to reveal the temperature profile inside the catalyst bed and compare the performance of a microchannel reactor with a conventional fixed bed reactor, a three-dimensional pseudo-homogeneous model was developed to describe the energy transfer and reactions. At steady state, partial

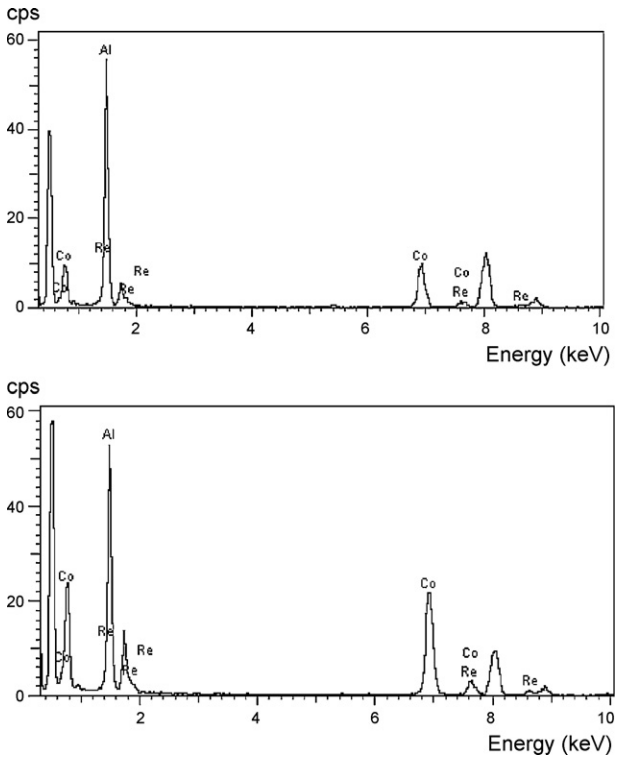

Fig. 8. (a) Energy dispersive X-ray spectroscopy (EDS/EDX) in Co dispersed region. (b) Energy dispersive X-ray spectroscopy (EDS/EDX) in Co segregated region.

differential equations describing conservation of mass and energy can be expressed as follows:

$$\nabla \cdot (-D_i \nabla c_i + c_i \vec{u}) = R_i$$

$$\nabla \cdot (-k \nabla T + \rho C_p T \vec{u}) = Q$$

where R_i is the formation rate of component i, which is function of component concentration (or partial pressure) and temperature; Q is the heat generation rate per unit volume of the catalyst bed, which is the function of reaction rate and heat of reaction; k is the effective conductivity of the catalyst bed; D is the effective diffusivity; $\vec{u}$ is linear velocity; c is species concentration; and T is temperature. The effective diffusivity is a combined effect of the molecular diffusion, Knudsen diffusion, and bed tortuosity. In the model, these parameters are associated with temperature, compositions, and catalyst properties. The effective thermal conductivity of the catalyst bed is of interest primarily for calculating the temperature in the bed during reaction. Supported metal on porous materials presents different thermal conductivity with different loading and synthesis methods. Empirical values from the literature have been taken to evaluate the synthesis process [30,31]. The model is constructed and solved with a commercial software FEMLAB package using the finite element approach.

Simulation compares the temperature profiles in a conventional tubular reactor with 0.635 cm i.d. and 2.54 cm catalyst packing height and in a microchannel reactor with the catalyst packing dimension of 1.27 cm × 0.0508 cm × 1.778 cm. Shown in Fig. 9, large temperature gradients exist in the furnace-heated conventional tubular reactor. At the same operating conditions (P = 20 atm, reactor wall temperature at 210 °C H_2/CO = 2, GHSV = 17,894 h^{-1}), the hot spot temperature can be as high as 239 °C in a tubular packed bed reactor. On the contrary, the microchannel catalyst slab bed shows a very uniform temperature profile, i.e., less than 1 °C temperature gradient. Although the

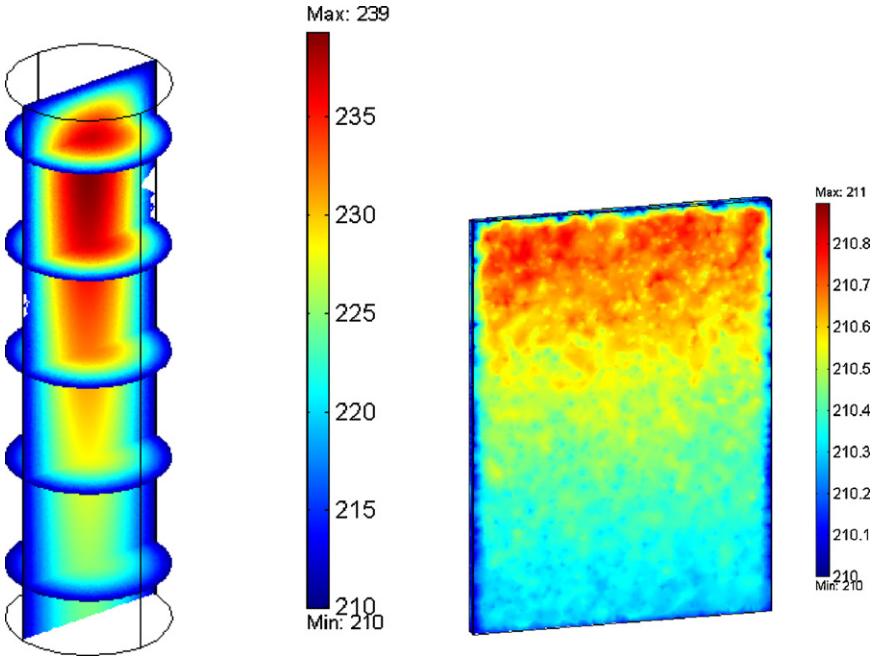

Fig. 9. Temperature profiles in a conventional tubular reactor and a microchannel reactor at the same operating conditions (P = 20 atm, reactor wall temperature at 210 °C, H_2/CO = 2, GHSV = 17,894 h^{-1}). Overall conversion level for the conventional tubular reactor is 62%, and 50% in the microchannel reactor (taken from reference [32]).

conversion level (62%) can be much higher in the conventional tubular reactor than that (50%) in a microchannel reactor since the catalysts "see" high average temperature in the tubular reactor, high methane selectivity in the tubular bed reactor occurs in the meantime and the hot spots may cause the metal sintering and result in fast catalyst deactivation. Such an exothermic effect is not significant when the reactor is operated at mild conditions such as low temperature or low space velocity with less heat duty. However, when a harsher condition occurs leading to high heat generation rate per unit volume, the catalyst bed temperature gradient will become large. Heat transfer capability in a tubular packed bed reactor is insufficient to mitigate such exothermic effects. On the other hand, the high heat transfer coefficient between the bed and wall, a large heat transfer surface area and short transfer distance in a microchannel reactor provide an essential isothermal conditions for FTS reactions. As shown in Fig. 10, at a GHSV of as high as 60,000 h^{-1} and the reactor wall temperature of 232 °C, the maximum temperature gradient in the microchannel reactor remains in a very narrow range (<3 °C). This gives a great potential to control methanation reaction and extend catalyst life.

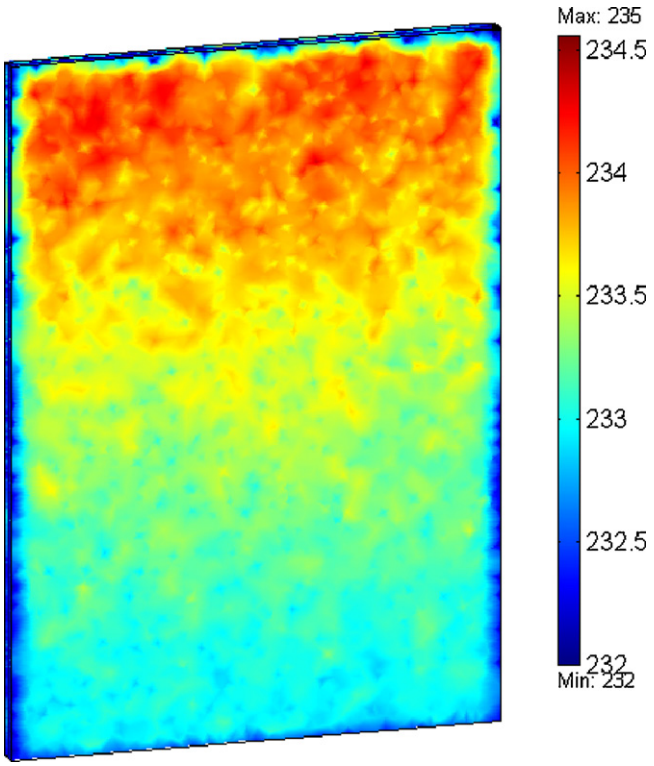

Fig. 10. Temperature distribution in a microchannel reactor with 60,000 h^{-1} GHSV and the reactor wall temperature at 232 °C.

Intraparticle transfer behavior was also studied for its effectiveness factor under the realistic Fischer–Tropsch reaction conditions. As a general estimation, material balance and energy balance in a finite shell of a particle gives that:

$$\Delta T = T - T_s = \frac{D_{eff}(-\Delta H)}{k_{eff}}(C_s - C)$$

This represents the correlation between concentration and temperature in one particle. When the reactants are converted completely inside of the catalyst particle, the maximum possible temperature difference is

$$\Delta T_{\max} = \frac{D_{eff}(-\Delta H)}{k_{eff}} C_s$$

It is clear that the temperature gradient is closely related to effective thermal conductivity and effective diffusivity besides heat of reaction. For Fischer–Tropsch synthesis, the max possible temperature gradient could be as high as 17 °C within a catalyst particle with 60 m^2/g surface area, 0.14 cm^3/g pore volume and 2.5 g/cm^3 particle density.

Although above analysis gives the worst scenario in non-isothermal effect for a certain reaction, the accuracy is poor since it is based on an assumption that the materials are all converted in the single particle. This assumption is not usually valid for many catalytic reaction systems. The prediction using above method will

overestimate the temperature gradient. Therefore, a more rigorous solution that takes into account of mass, energy transfer and reaction kinetics is necessary to analyze the intraparticle temperature gradient. Continuity equations of mass and energy are written as follows:

$$u \cdot \nabla c = D_{eff} \nabla^2 c + (-r)$$

$$\rho c_p u \cdot \nabla T = k_{eff} \nabla^2 T + (-r)(-\Delta Hr)$$

In spherical coordinates, boundary conditions in scalar forms are

$$\left.\frac{\partial T}{\partial r}\right|_{r=0} = 0$$

$$\left.\frac{\partial c}{\partial r}\right|_{r=0} = 0$$

$$T(r = R) = T_s$$

$$c(r = R) = c_s$$

The effective diffusivity is a combined effect of the bulk and Knudsen diffusion, which is function of temperature, compositions and catalyst properties. Numeric solution in FEMLAB gives the result in our benchmark testing condition: T(particle surface) = 232 °C, GHSV = 21,500 h^{-1}, H_2/CO = 2, total conversion = 60%, particle property: d_p = 150 μm, ρ_p = 2.5 g/cm^3, k_{eff} = 0.2 W/m K. Fig. 11 shows the temperature distribution in a single particle. It is found that a 150 μm catalyst particle is virtually isothermal during the FT synthesis reactions. The max temperature difference in the particle is less than 0.2 °C. Simulation results also indicate that particle size contributes greatly to the intraparticle non-isothermal effect. Shown in Fig. 12, changing particle size but maintaining the same other conditions as above yield various temperature gradients. For example, a 1 mm catalyst particle will give an intraparticle temperature gradient as high as 6 °C. Moreover, the shell-egg type temperature distribution in such a case is less uniform compared to that of the 150 μm particles due to the severer transport limitation (both mass diffusion and heat conduction).

As a criteria check, the effectiveness factor of the spherical shaped catalyst particle is related to Thiele Modules Φ and two other dimensionless factors β and γ defined as follows [30]:

$$\beta = \frac{D_{eff}(-\Delta H)}{\lambda_p T_s} C_s$$

$$\gamma = \frac{E}{RT_s}$$

$$\Phi = R\sqrt{\frac{k}{D_{eff}}}$$

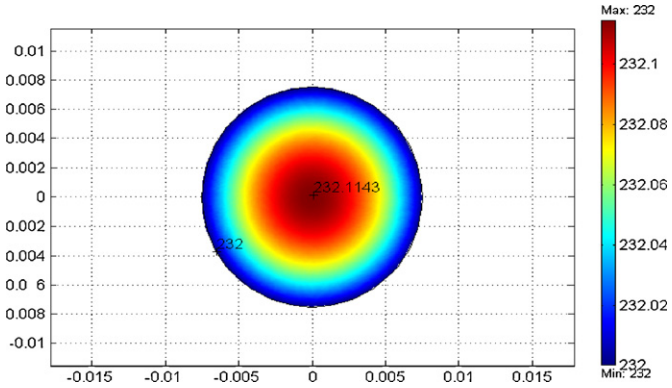

Fig. 11. Temperature distribution in a single particle. T(particle surface) = 232 °C, GHSV = 21,500 h^{-1}, H_2/CO = 2, total conversion = 60%, particle property: d_p = 150 μm, ρ_p = 2.5 g/cm^3, k_{eff} = 0.2 W/m K.

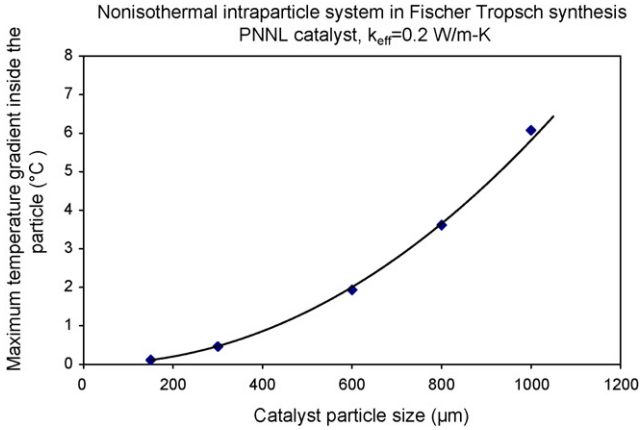

Fig. 12. Intraparticle temperature gradient versus catalyst particle size.

The benchmark condition with a particle size of 150 μm gives Thiele number Φ as small as 0.003, β as 0.08, and γ as 24. The effectiveness factor is close to unity by applying criteria developed by Anderson (1963) [33] and Peterson (1965) [34]. This independently verifies the modeling results. Therefore, in our benchmarked testing conditions with small catalyst particle sizes (45 and 150 μm) used in the microchannel reactor, intraparticle transport provides an isothermal system for Fischer–Tropsch synthesis reactions.

4. Conclusion

A microchannel catalytic reactor was used to evaluate catalyst performance in Fischer–Tropsch synthesis. This reactor provides effective heat removal and improved mass transfer characteristics for the exothermic reactions. Integrated with a highly active and selective catalyst, such a reactor allows synthesis process to be operated at high gas hourly space velocity as high as 60,000 h^{-1} and gives productivity as high as 2.14 g C_{2+}/(g-cat h) while still maintaining low methane selectivity and high chain growth probability. A considerable improvement in suppressing methane formation was observed with the smaller catalyst particles. It was found that high-pressure operation in a microchannel reactor significantly reduces methane formation and increases chain growth probability (α). It was also found that CO conversion increases with H_2/CO ratio, while methane selectivity decreases.

Acknowledgments

The authors gratefully acknowledge the support of US DOE EERE, Office of the Biomass Program. This work was performed in the Environmental Molecular Sciences Laboratory, a national scientific user facility sponsored by the US Department of Energy's Office of Biological and Environmental Research and located at Pacific Northwest National Laboratory in Richland, WA. We also would like to thank Dr. Chongmin Wang for his help on TEM.

References

[1] M.A. Agee, in: A. Parmaliana, et al. (Eds.), Natural Gas Conversion V, Elsevier Science B.V., Amsterdam, 1998, p. 931.
[2] M.M. Carson, M.A. Carson, M.A. Roberts, Oil Gas J. 19 (June) (1995) 33.
[3] M.M.G. Sendfden, A.D. Punt, A. Hoek, in: A. Parmaliana, et al. (Eds.), Natural Gas Conversion V, Elsevier Science B.V., Amsterdam, 1998, p. 961; A. Hoek, Cat-Con2003, Houston, May 5, 2003.
[4] V.M.H. Van Wechem, M.M.G. Senden, in: H.E. Curry-Hyde, R.F. Howe (Eds.), Natural Gas Conversion II, Elsevier Science B.V., Amsterdam, 1994, p. 43.

[5] V.K. Venkataraman, H.D. Guthrie, R.A. Avellanet, D.J. Driscoll, in: A. Parmaliana, et al. (Eds.), Natural Gas Conversion V, Elsevier Science B.V., Amsterdam, 1998 p. 913.
[6] C. Knottenbelt, Catal. Today 71 (2002) 437.
[7] E. Iglesia, Appl. Catal. A: Gen. 161 (1997) 59.
[8] A. Khodakov, W. Chu, P. Fongarland, Chem. Rev. 107 (5) (2007) 1692.
[9] I. Arslan, J.C. Walmsley, E. Rytter, E. Bergene, P.A. Midgley, J. Am. Chem. Soc. 130 (17) (2008) 5716.
[10] G.L. Bezemer, J.H. Bitter, H.P.C.E. Kuipers, H. Oosterbeek, J.E. Holewijn, X. Xu, F. Kapteijn, A. Jos van Dillen, K.P. de Jong, J. Am. Chem. Soc. 128 (12) (2006) 3956.
[11] A.M. Saib, A. Borgna, J. Van de Loosdrecht, P.J. Van Berge, J.W. Geus, J.W. Niemantsverdriet, J. Catal. 239 (2) (2006) 326.
[12] M.E. Dry, Appl. Catal. A: Gen. 138 (1996) 319.
[13] S.T. Sie, R. Krishna, Appl. Catal. A: Gen. 186 (1999) 55.
[14] B.H. Davis, Catal. Today 71 (2002) 249.
[15] D.J. Duvenhage, T. Shingles, Catal. Today 71 (2002) 301.
[16] M.E. Dry, Catal. Today 71 (2002) 227.
[17] F. Fischer, H. Tropsch, Brennstoff-Chem. 7 (1926) 299.
[18] R.B. Anderson, The Fischer–Tropsch Synthesis, Academic Press, London, 1984, p. 2.
[19] H.H. Storch, N. Golumbic, R.B. Anderson, The Fischer–Tropsch and Related Syntheses, Wiley, New York, 1951.
[20] M.J. Baird, R.R. Schehl, W.P. Haynes, J.T. Cobb, Ind. Eng. Chem., Prod., Res. Dev. 19 (1980) 175.
[21] C.D. Frohning, in: J. Falbe (Ed.), New Syntheses with Carbon Monoxide, Springer, New York, 1980, p. 309.
[22] S.C. Saxena, Catal. Rev.: Sci. Eng. 37 (1995) 227.
[23] G.P. Van Der Lann, A.A.C.M. Beenackers, Catal. Rev.: Sci. Eng. 41 (3–4) (1999) 255.
[24] K. Jahnisch, V. Hessel, H. Lowe, M. Baerns, Angew, Chem. Int. Ed. 43 (2004) 406.
[25] J.D. Holladay, Y. Wang, E.O. Jones, Chem. Rev. 104 (2004) 4767.
[26] G. Kolb, V. Hessel, Chem. Eng. J. 98 (2004) 1.
[27] C. Cao, G. Xia, J.D. Holladay, E.O. Jones, Y. Wang, Appl. Catal. A: Gen. 262 (2004) 19.
[28] E. Iglesia, S.C. Reyes, S.L. Soled, in: E.R. Becker, C.J. Pereira (Eds.), Computer-aided Design of Catalysts and Reactor, Marcel Dekker, New York, 1993, p. 199.
[29] I.C. Yates, C.N. Satterfield, Energy Fuels 5 (1991) 168.
[30] C.N. Satterfield, Heterogeneous Catalysis in Industrial Practice, 2nd ed., McGraw-Hill, Inc., p. 511.
[31] R.A. Sehr, Chem. Eng. Sci. 9 (1958) 145.
[32] C. Cao, D.R. Palo, A.L.Y. Tonkovich, Y. Wang, Catal. Today 125 (2007) 29.
[33] J.B. Anderson, Chem. Eng. Sci. 18 (1958) 147.
[34] E.E. Peterson, Chemical Reaction Analysis, Prentice-Hall, 1965.